Available online at www.sciencedirect.com
SCIENCE DIRECT
Journal of Catalysis 237 (2006) 314–321
JOURNAL OF CATALYSIS
www.elsevier.com/locate/jcat

TiO_2-loaded Cr-modified molecular sieves for 4-chlorophenol photodegradation under visible light

Bo Sun, Ettireddy P. Reddy, Panagiotis G. Smirniotis *

Department of Chemical and Materials Engineering, University of Cincinnati, Cincinnati, OH 45221-0012, USA

Received 2 September 2005; revised 24 October 2005; accepted 30 October 2005

Available online 13 December 2005

Abstract

Here we report the aqueous photodegradation of 4-chlorophenol under visible light (wavelength >400 nm) with three kinds of mesoporous molecular sieves (MCM-41, MCM-48, and SBA-15) incorporated with Cr and TiO_2 (TiO_2/Cr-MS). The Si/Cr atomic ratios in the synthesized materials are 80, 40, and 20, respectively. These materials are characterized with BET surface area, pore size distribution, X-ray diffraction (XRD), ultraviolet–visible light (UV–vis) spectra, and temperature-programmed reduction (TPR). UV–vis and TPR results indicate that the Cr is present as Cr^{6+} in all Cr-MS and TiO_2/Cr-MS samples. The TPR results further indicate that an Si–O–Cr–O–Si bond structure is formed in the MCM-41 matrix, bulk Cr oxide exists outside the MCM-48 matrix, and Cr interacts mainly with silica on the surface of SBA-15. The incorporation of Cr extends the light absorption edge of TiO_2/Cr-MS to 550 nm. The activities of TiO_2/Cr-MS with different molecular sieves are compared for aqueous photodegradation of 4-chlorophenol under visible light. It is found that the molecular sieve plays an important role in photocatalyst activity and that MCM-41 is the support producing the best photocatalyst. The interaction of Cr^{6+} and TiO_2 allows for a special transition under visible light, $Cr^{6+}{=}O^{2-} \rightarrow Cr^{5+}{-}O^{1-}$, and is essential for the activity of a photocatalyst under visible light.

Keywords: Titania; SBA-15; MCM-41; MCM-48; Deactivation; Reactivation; Oxidation state

1. Introduction

Heterogeneous photodegradation of organic pollutants with titanium dioxide has drawn the attention of researchers for its efficiency and promises of economy [1–4]. TiO_2 in the anatase phase is the most widely studied photocatalyst, but it can only work only under ultraviolet (UV) light (wavelength <387 nm) for its band gap of 3.2 eV [5,6]. Rutile TiO_2 has been claimed to be inactive or much less active, although it has a smaller band gap of 3.0 eV (wavelength <413 nm). Only 4% of the solar energy reaching the Earth's surface is UV light [7]. To utilize the full spectrum of solar light, a number of modifications have been tried, mainly on TiO_2, to make a catalyst work under visible light [7–16].

The photodegradation rate with supported titanium dioxide can be higher than that with neat titania [17,18]. Doping TiO_2 with metal ions may enhance its photoactivity [19,20] or even may enable its sensitization under visible light [13–16]. Our earlier studies involving TiO_2-loaded transition metal-incorporated MCM-41 [13–16], found that only TiO_2-loaded, Cr-incorporated MCM-41 worked under visible light. UV–vis spectra showed that incorporated Cr extended the light absorption of TiO_2 into the visible range, and TPR revealed a clear interaction between Cr^{6+} and TiO_2, which was proposed to be the reason for the catalyst's photoactivity under visible light [16]. The MCM-41 structure was shown to enhance the Cr–TiO_2 interaction compared with bulk silica oxides. The present study compares MCM-41 [21], MCM-48 [22], and SBA-15 [23] as supports for Cr incorporation and TiO_2 loading; the results clarify the effect of molecular structure on photocatalyst activity.

* Corresponding author. Fax: +1 513 556 3473.
E-mail address: panagiotis.smirniotis@uc.edu (P.G. Smirniotis).

0021-9517/$ – see front matter
doi:10.1016/j.jcat.2005.10.028

2. Experimental

2.1. Synthesis of 25 wt% TiO_2-loaded Cr-modified SBA-15, MCM-48, MCM-41, and silica bulk oxide specimens

2.1.1. Cr-modified MCM-41 (Cr-MCM-41)

The Cr-modified MCM-41 specimen was prepared as reported previously [16]. First, 3 ml of deionized (DI) water was added to 35 ml of Ludox HS-40 colloidal silica (40%) under stirring, and then 30.32 ml of 25% tetramethylammonium hydroxide (Aldrich, 25%) was added. Independently, 18.25 g of cetyltrimethylammonium bromide (CTABr, Alfa Aesar) was dissolved in 33 ml of water, and subsequently 7 ml of ammonium hydroxide (Fisher, 29.6%) was introduced when the CTABr solution became a transparent gel and could be magnetically stirred again after gelation. Then the latter solution was transferred to the first solution. For synthesis of Cr-MCM-41 with an atomic Si/Cr ratio of 80 (or 40 or 20) [16], a specific amount of $CrCl_3 \cdot 6H_2O$ (Fisher) was dissolved in 20 ml of water and added dropwise to the resulting mixture. The final mixture was stirred for 2 h at 80 °C, then transferred into a Teflon bottle and treated under autogenous pressure without stirring at 100 °C for 3 days. The resulting solids were filtered, washed, and dried in air. The dried powder was calcined at 550 °C for 10 h under a moderate air flow with a temperature ramp of 2 °C/min.

2.1.2. Cr-modified MCM-48 (Cr-MCM-48)

The pure siliceous MCM-48 was synthesized as described previously [24]. In a typical synthesis, 17.5 g of CTABr and 1.92 g of sodium hydroxide were dissolved in 99 ml of DI water, and then 20.8 g of tetraethyl orthosilicate (TEOS) (Aldrich) was added into the mixture. The molar composition of the gel was TEOS: 0.48 NaOH: 0.48 CTAB: 55 H_2O. For the synthesis of Cr-MCM-48 with an atomic Si/Cr ratio of 80 (or 40 or 20), a specific amount of $CrCl_3 \cdot 6H_2O$ was dissolved in 10 ml of DI water, then added dropwise into the solution after TEOS was added. The remaining steps were identical to those followed for pure siliceous MCM-48 synthesis. The gel was stirred at room temperature for about 1 h and then transferred into a Teflon bottle and treated under autogenous pressure without stirring at 100 °C for 3 days. The resulting solution was cooled to room temperature, and its pH was adjusted to 7.0 by adding HCl. Then it was heated at 373 K for another 2 days. The final materials were filtered, washed, dried at ambient temperature, and calcined at 550 °C for 6 h under flowing air at heating rate of 2 °C/min.

2.1.3. Cr-modified SBA-15 (Cr-SBA-15)

The pure siliceous SBA-15 was synthesized as described previously [25]. In a typical synthesis, 12.0 g of Pluronic P123 (Aldrich) was dissolved in 60 ml of hydrochloric acid (35–37%) and 312 ml of DI water, and the solution was heated to 308 K during stirring. Then 25.6 g of TEOS (Aldrich) was added to the mixture. The resulting solution was kept at 35 °C for 24 h, after which the final gel was put into a Teflon bottle, which was placed in an oven and heated at 100 °C for 48 h. The resulting materials were filtered, washed, dried at ambient temperature, and calcined at 500 °C for 6 h under flowing air at a heating rate of 1 °C/min.

A method of adding $CrCl_3 \cdot 6H_2O$ directly after adding TEOS failed to produce Cr-SBA-15 simply because all of the Cr came out with the water in the subsequent filtration step, and Cr cannot enter the silica structure with this method. The acidic conditions for preparation of SBA-15 is unfavorable for incorporation of metal species. An incipient wetness method [26] was used in Cr-SBA-15 synthesis. A specific amount of $Cr(NO_3)_3 \cdot 9H_2O$ (Fisher) corresponding to the Si/Cr atomic ratio of 80 (or 40 or 20) was dissolved in 150 ml of distilled water, and 1.5 g of SBA-15 was added to the solution later. The suspension was stirred and dried at 70 °C. The resulting powder was calcined at 550 °C for 6 h under moderate air flow with a temperature ramp of 1 °C/min.

2.1.4. TiO_2 loading on the Cr-modified molecular sieves (TiO_2/Cr-MS)

The resulting Cr-modified MCM-41, MCM-48, and SBA-15 samples prepared as described earlier (typically 1.0 g) were dispersed in 100 ml of isopropyl alcohol (Pharmco, 99.8%). Then 1.28 mL of titanium (IV) isopropoxide (Aldrich, 97%) was added to achieve 25 % loading [13,18]. The samples were dried while being stirred at ambient temperature, and then calcined at 450 °C for 3 h at a heating rate of 2 °C/min.

2.2. Characterizations

2.2.1. XRD

All Cr-MS and TiO_2/Cr-MS materials prepared were characterized using Nicolet powder X-ray diffractometer equipped with a Cu-K_α source to assess their structure and crystallinity. The synthesized Cr-MCM-41, Cr-MCM-48, TiO_2/Cr-MCM-41, and TiO_2/Cr-MCM-48 samples were run with 2θ changing from 2° to 7° to assess the structure of the MS matrix. Cr-SBA-15 and TiO_2/Cr-SBA-15 were run with 2θ changing from 1.5° (XRD machine's limit) to 3° to assess the structure of the SBA-15 matrix. TiO_2/Cr-MS were also run with 2θ changing from 20° to 50° to assess the crystallinity of the TiO_2 loaded.

2.2.2. BET surface area and pore size distribution

BET surface area and pore size distribution studies were conducted at −196 °C using Micromeritics ASAP 2010 apparatus to characterize the synthesized photocatalysts. Samples of 0.05–0.06 g were degassed at 300 °C for at least 10 h in the degassing port of the apparatus. The surface area was calculated from adsorption isotherms by the BET method, and the pore size was obtained from the adsorption branch of the isotherm using the BJH method. The results obtained are listed in Table 1.

2.2.3. UV–vis spectra

The prepared materials were characterized by a UV–vis spectrophotometer (Shimadzu 2501PC) with an integrating sphere attachment (ISR1200) for their diffuse reflectance in the

Table 1
Physical characterization results for Cr-MS and 25%TiO_2/Cr-MS materials utilized in the present study

Molecular sieves (Si/Cr)	Cr-modified molecular sieves				After TiO_2 loading			
	BET[a] surface area (m^2/g)	Pore volume[a] (cm^3/g)	Pore size[a] (Å)	Unit cell parameter[b] (Å)	BET[a] surface area (m^2/g)	Pore volume[a] (cm^3/g)	Pore size[a] (Å)	Unit cell parameter[b] (Å)
MCM-41	1143	1.03	35	43	890	0.77	32	41
MCM-41 (80)	999	0.99	40	42	777	0.65	32	41
MCM-41 (40)	912	0.95	40	43	712	0.60	37	43
MCM-41 (20)	664	1.14	69	43	547	0.81	57	42
MCM-48	983	0.65	26	89	786	0.47	22	85
MCM-48 (80)	887	0.81	35	89	571	0.50	33	89
MCM-48 (40)	739	0.65	33	92	496	0.45	34	90
MCM-48 (20)	490	0.63	50	97	393	0.46	44	97
SBA-15	827	1.21	57	117	634	0.86	53	113
SBA-15 (80)	681	1.03	58	112	528	0.71	52	115
SBA-15 (40)	685	1.04	59	114	510	0.67	51	115
SBA-15 (20)	669	0.97	56	113	478	0.63	51	114

[a] Measured by physisorption with liquid nitrogen.
[b] Unit cell parameter $= 2d_{100}/\sqrt{3}$ (MCM-41) [21]; unit cell parameter $= \sqrt{6}d_{211}$ (MCM-48) [28]; unit cell parameter $= 4d_{200}/\sqrt{3}$ (SBA-15) [29].

range of wavelengths of 200–900 nm. $BaSO_4$ was used as the standard in these measurements.

2.2.4. TPR measurement

The TPR was carried out in a temperature range of 50–550 °C on a Micromeritics Autochem 2910 instrument with a temperature ramp of 2 °C/min. The samples were pretreated at 200 °C with ultrahigh-purity O_2 (Matheson) for 2 h. A total of 10 ml/min of 10% H_2 in Argon (Matheson) was passed through the sample tube during the measurement.

2.3. Visible light photocatalytic performance experiments

The photocatalytic testing included the degradation of 4-chlorophenol (4-CP, Aldrich, used as the probe molecule), which was performed in a batch-type round flat-plate reactor described previously [13]. The irradiation source was a 450-W medium-pressure mercury lamp (Jelight, J05PM1HGC2). A double Acrylic OP-2 (Museum quality) sheet was placed between the light source and the reactor for the purpose of excluding ultraviolet radiation (wavelength <400 nm). The cooling jacket around the reactor allowed to effectively preclude the infrared part of the spectrum from penetrating into the reaction solution and cooled the lamp. The local light intensity on the sheet was 7×10^{-5} W cm^{-2}, as measured with a detector (International Light, model SED033 #3435) connected to a radiometer (International Light, model IL 1700). The temperature for reaction was kept at 25 ± 0.5 °C. Then 500 ml of 1 mM 4-CP was stirred with 400 mg of 25%TiO_2-loaded catalyst for 30 min. The pH of the reaction suspension was not adjusted. The suspended catalyst in aqueous system was oxygenated (Wright Brothers, 99.9%) at 0.5 L/min to ensure complete saturation. The samples of reaction suspension were taken with a syringe at different intervals and filtered with Cameo 25P polypropylene syringe filters (OSMONICS, catalog no. DDP02T2550). The sample solutions were analyzed with a total organic carbon analyzer (TOC-VCSH, Shimadzu).

3. Results and discussion

3.1. BET surface area and pore size/volume

All of the final Cr-MS and TiO_2/Cr-MS samples after calcination were yellow, indicating that the Cr^{3+} impregnated in the catalyst was oxidized into Cr^{6+}. The BET surface area of Cr-MCM-41 (Table 1) decreased from 1143 to 664 m^2/g with Si/Cr changing from ∞ to 20. A similar trend occurred with Cr-MCM-48. The decreased surface area with Cr incorporation can be explained by the incompatibility of the Cr^{6+} and Si^{4+} size and structure in the oxide compound. The radii of Cr^{6+} in an octahedral structure was 58 pm, whereas that of Si^{4+} in the same structure was 54 pm. More MCM-41 and MCM-48 structures tend to collapse with increasing Cr incorporation, increasing the pore sizes of both Cr-MCM-41 and Cr-MCM-48 [13–18,27]. The surface area and pore size distribution of all Cr-SBA-15 samples were approximately the same, because Cr was impregnated after formation of the SBA-15 matrix structure. But the BET surface area of Cr-SBA-15 was about 150 m^2/g less than that of pure SBA-15. The loading of 25%TiO_2 on Cr-MS generally resulted in a decrease in BET surface area of about 200 m^2/g. At the same time, pore volume decreased by about 0.3 cm^3/g and pore size also decreased, clearly indicating that TiO_2 entered the Cr-MS pores. In comparison, the unit cell sizes of Cr-MS samples were approximately the same after TiO_2 loading (Fig. 1 and Table 1), proving that the MS matrix structure remains the same.

3.2. XRD characterization

The XRD peak intensity of Cr-MS decreased with the amount of Cr incorporated (Fig. 1). The trend of the peak intensity with respect to the amount of Cr incorporation was consistent with the change of BET surface area and pore volume. The unit cell parameters of Cr-MCM-41 [21], Cr-MCM-48 [28], and Cr-SBA-15 [29] were about 42A, 90A, and 113A, respectively. The corresponding unit cell parameters of the TiO_2/Cr-MS

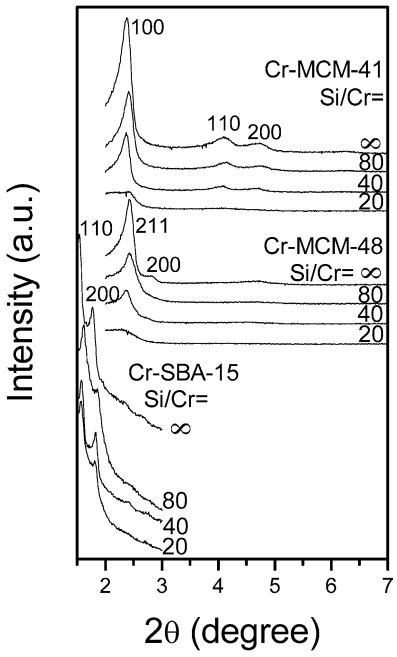

Fig. 1. XRD of Cr-modified MCM-41, MCM-48 and SBA-15.

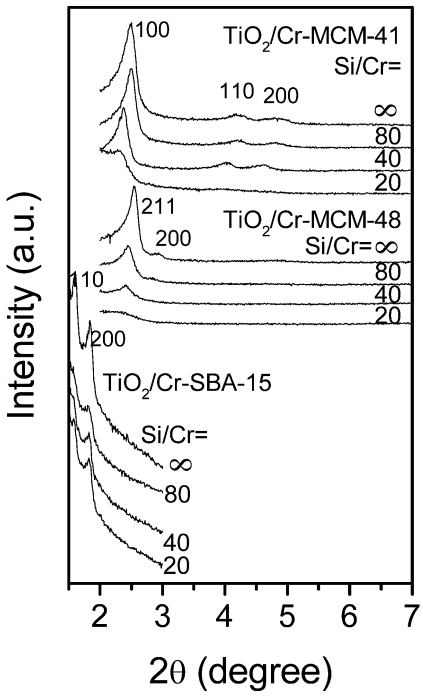

Fig. 2. XRD of 25% TiO_2-loaded Cr-modified MCM-41, MCM-48 and SBA-15.

samples with different Si/Cr ratios maintained nearly the same trend as those of the Cr-MS samples (Figs. 1 and 2). The weak peaks in the XRD curves (not shown) from 20° to 50° indicate that the titania inside the MCM-41 structure is mostly amorphous.

3.3. UV–vis characterization

Cr incorporation enabled the three molecular sieves to absorb visible light with a wavelength <550 nm (Fig. 3). Two light absorption peaks, corresponding to Cr^{6+}, appeared at 274 and 360 nm for all Cr-MS samples with varying Si-to-Cr ratios. The heights of the two peaks grew as Si/Cr decreased from ∞ to 20, then decreased with further Cr incorporation. A shoulder occurred at 430 nm for Cr-MCM-41 (Si/Cr = 80, 40) and Cr-MCM-48, which also corresponds to the existence of Cr^{6+}. This shoulder is disguised by the ramp of the peak at 360 nm in the curves for Cr-MCM-41 (Si/Cr = 20) and Cr-SBA-15. The loading of TiO_2 increases the light absorption ability of the samples, especially in the UV range. Comparing the UV–vis spectra (Figs. 3 and 4) reveals that all of the visible light absorbance of the final TiO_2/Cr-MS corresponds to the peaks appearing in the Cr-MS samples. The peaks of Cr^{6+} at 274 and 360 nm simply become shoulders after TiO_2 loading; the length of the shoulders increase with increasing Cr amount for each MS. This is consistent with the trend of peak height shown in Fig. 3. The shoulder at 430 nm in Fig. 3 is disguised in the spectra of TiO_2/Cr-MCM-41and TiO_2/Cr-SBA-15. The visible light (400–500 nm) absorbance of the final catalysts increases with the amount of Cr incorporated with each series of MS.

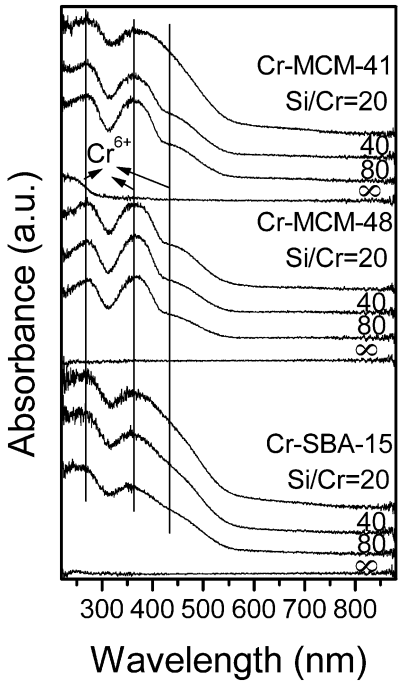

Fig. 3. UV–vis spectra of Cr-modified MCM-41, MCM-48 and SBA-15.

3.4. TPR characterization

The TPR curves of Cr-MS and TiO_2/Cr-MS are shown in Figs. 5 and 6, respectively. The TPR peaks of Cr-MCM-41 appear at around 350 °C, due mainly to the reduction of incorporated Cr^{6+} in MCM-41 to Cr^{3+}, and the reduction starts at around 225 °C [16] (Fig. 5). The intensity of the peak increases with increasing Cr concentration without a change in

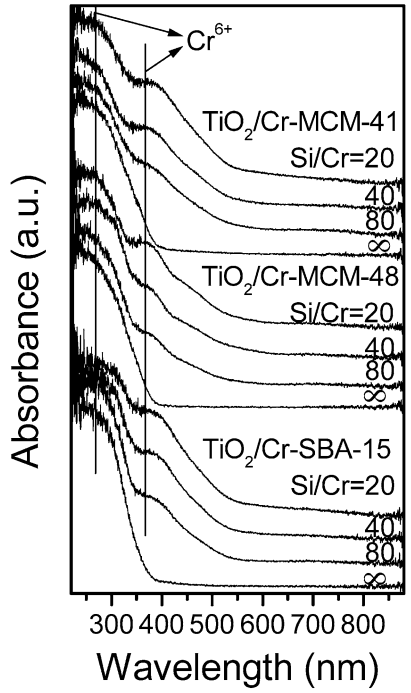

Fig. 4. UV–vis spectra of 25% TiO_2-loaded Cr-modified MCM-41, MCM-48 and SBA-15.

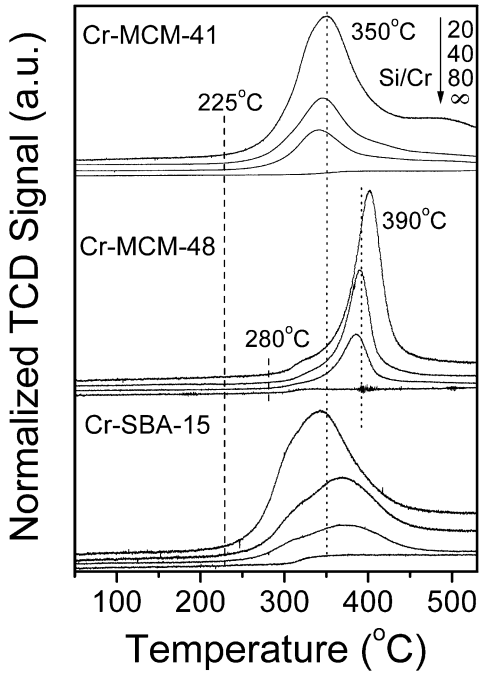

Fig. 5. TPR curves of Cr-modified MCM-41, MCM-48 and SBA-15.

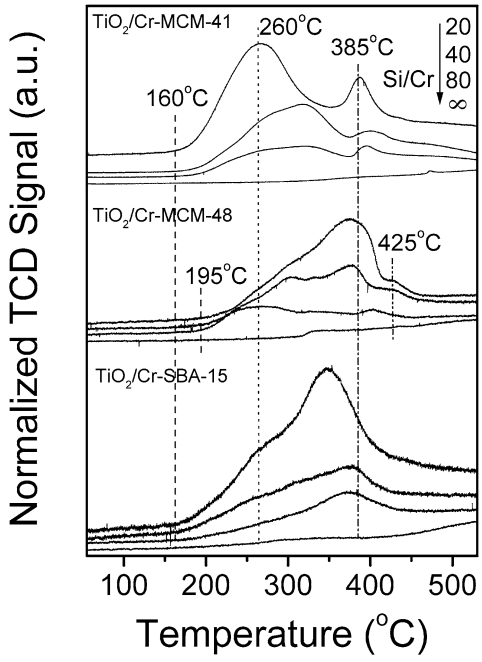

Fig. 6. TPR curves of 25% TiO_2-loaded Cr-modified MCM-41, MCM-48 and SBA-15.

the reduction temperature. In the case of Cr-MCM-48, the reduction of Cr starts at around 280 °C, and the TPR peaks appear at around 390 °C, similar to the case of pure CrO_3 reducing from Cr^{6+} to Cr^{3+} (Fig. S1 in supplementary material). This indicates that most of the Cr in MCM-48 remains as bulk chromium oxide. As shown in Fig. 5, a broad reduction peak of Cr appears at 370 °C with Cr-SBA-15 (Si/Cr = 80, 40) and decreases with increasing Cr loading. This finding demonstrates that the chromium exists as isolated species at lower loadings and highly dispersed states of chromium at higher loadings. This trend is not observed with Cr-MCM-41 and Cr-MCM-48, because the wet impregnation method is used in Cr-SBA-15 synthesis, whereas in situ Cr incorporation is used for Cr-MCM-41 and Cr-MCM-48 synthesis. The difference also results from the differing Cr structure in these three mesoporous materials. The Si–O–Cr–O–Si bond structure is formed in the MCM-41 matrix (Scheme 1a), bulk Cr oxide exists outside the MCM-48 matrix (Scheme 1b), and Cr interacts mainly with silica on the surface of SBA-15 (Scheme 1c). This difference may be due to the three-dimensional (3D) pore structure of MCM-48 [30] compared with the linear structure of MCM-41 and SBA-15. The peak height and area increase with increasing Cr amount for each molecular sieve. The total H_2 consumed by both Cr-MCM-41 and Cr-SBA-15 are the same. It is higher than the total H_2 consumed by Cr-MCM-48, possibly because part of the Cr is wrapped up by the 3D structure of MCM-48.

TiO_2 loading changes the TPR curves of Cr-MS (Fig. 6). The interaction between Cr and TiO_2 lowers the starting reduction temperature of Cr-MCM-41 and Cr-SBA-15 by about 65 °C and that of Cr-MCM-48 by 85 °C. At the same time, the temperature span for reduction increases. Two peaks appear in the TPR curves of TiO_2/Cr-MCM-41. The first of these peaks (at 260 °C) is due to the reduction of Ti^{4+} and Cr^{6+} (Si–O–Cr), which are interacting with each other. The comparison between the TPR curves of the samples with and without TiO_2 loading implies that the second peak (at 385 °C) is due to Cr^{6+} free from interacting with the deposited TiO_2. The atomic ratio of Ti to Cr changes from 20.1 to 5.0 when the Si/Cr ratio decreases from 80 to 20; thus there are much more Ti atoms than Cr atoms in TiO_2/Cr-MS. Little Cr^{6+} exists free from

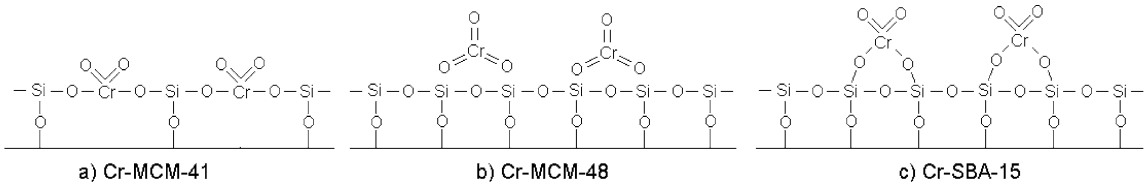

Scheme 1.

TiO_2 (corresponding to the second peak) with TiO_2/Cr-MCM-41, indicating that TiO_2 is well deposited on the surface of the MCM-41 structure. This layer of TiO_2 stops a fraction of Cr^{6+} in the framework from being reduced by H_2, as indicated by the decreased peak intensity in TPR after TiO_2 loading. One new shoulder peak appears at around 260 °C along with the original reduction peaks of Cr-SBA-15 after TiO_2 loading. This shoulder, which is due to the interaction of Cr and TiO_2, is much smaller than that of TiO_2/Cr-MCM-41. But the total H_2 consumed by both TiO_2/Cr-MCM-41 and TiO_2/Cr-SBA-15 remains the same (Fig. 7). This is because the Cr is added into SBA-15 after formation of the SBA-15 silica structure and the Cr in MCM-41 is incorporated in situ during formation of the MCM-41 structure. Thus, the later addition of Cr may corrugate the inner surface of SBA-15 pores after calcination, preventing the titania source from efficiently entering the pores and resulting in a large proportion of Cr^{6+} in SBA-15 being free from TiO_2. In comparison, the in-situ Cr incorporation in MCM-41 eliminates this possibility by forming a smooth surface with the Si–O–Cr structure in matrix. Thus, TiO_2 can interact efficiently with Cr. The inheritance of no Si–O–Cr bond (Scheme 1b) by TiO_2/Cr-MCM-48 results in a different starting reduction edge (195 °C) than that for TiO_2/Cr-MCM-41 and TiO_2/Cr-SBA-15. This indicates that the first peak in TPR curve of TiO_2/Cr-MCM-48 is due to the interaction of Ti^{4+} and Cr^{6+} free from silica structure. The second peak (at 385 °C) and third peak (at 435 °C) are due to stepwise reduction (Cr^{6+} to Cr^{3+}) of the CrO_3, which is untouched by TiO_2. The total H_2 consumed by either the Cr-MS or TiO_2/Cr-MS catalyst sample during TPR studies increases almost linearly with an increasing Cr amount from 80 to 20 (Fig. 7), implying that the oxidation states of Cr in all of these catalysts are the same. In combination with UV–vis spectra, Cr exists as Cr^{6+} in these catalysts.

3.5. Catalytic activity

Fig. 8a shows the curves of total carbon concentration with respect to time during 4-CP photodegradation under visible light. All the catalysts deactivate in the visible light. The deactivation mechanism was proposed to be that Cr^{6+} is reduced to Cr^{5+} little by little [13,31]. The photo-oxidation of organic compounds follows a Langmuir–Hinshelwood rate form [32]. When the reactant concentration is high, the reaction form is zero order [33–35]. Initial TOC removal rate and total TOC removal are calculated to characterize quantitatively the catalyst activity (Figs. 8b and c). Initial TOC removal rate is the slope of TOC curve (Fig. 8a) at the beginning of the photoreaction, and total TOC removal is the TOC removed from the

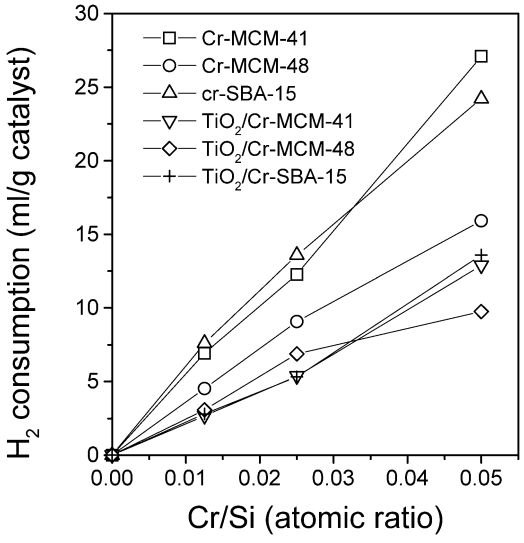

Fig. 7. Total H_2 consumption during TPR analysis of Cr-modified and 25% TiO_2-loaded Cr-modified MCM-41, MCM-48 and SBA-15.

beginning of the reaction to the catalyst deactivation. The initial TOC removal rate with TiO_2/Cr-MCM-41 increases almost linearly with Cr/Si ratio, but those with TiO_2/Cr-MCM-48 and TiO_2/Cr-SBA-15 follow different trends. The photoactivity shown with TiO_2/Cr-MCM-48 also indicates that the Si–O–Cr structure is not necessary for an active photocatalyst, and the interaction of TiO_2 and Cr^{6+} is essential for a photocatalyst to be active. But the Si–O–Cr structure is important for achieving a more active photocatalyst (TiO_2/Cr-MCM-41 with an Si-to-Cr ratio of 20). As we explained previously [13], the presence of a tetrahedrally coordinated Cr^{6+} of the catalyst is essential, because its fully reduced form does not exhibit any photoactivity. However, the role of Cr^{3+} is still unclear and the deactivated catalyst was rich in Cr^{3+}. The CrO_3-doped glasses [36], as well as porous molecular sieves [37–40], are known for their tetrahedral coordination of chromium. Such coordination was also observed with extended X-ray fine structure and photoluminescence studies [37–44]. This structure allows for a special transition under visible light: $Cr^{6+} = O^{2-} \leftrightarrow Cr^{5+}–O^{1-}$. Such a transition, when it occurs in contact with amorphous TiO_2, can produce an effect similar to that found in platinum (IV) chloride-modified amorphous titania [12]. Total TOC removal increases linearly with increasing Cr amount for each TiO_2/Cr-MS. The total removal with TiO_2/Cr-SBA-15 is a little less than that with TiO_2/Cr-MCM-41, and both of these are much greater than that with TiO_2/Cr-MCM-48. This clearly indicates that a proportion of Cr in the 3-D MCM-48 pore structure is not accessible for the photoreaction.

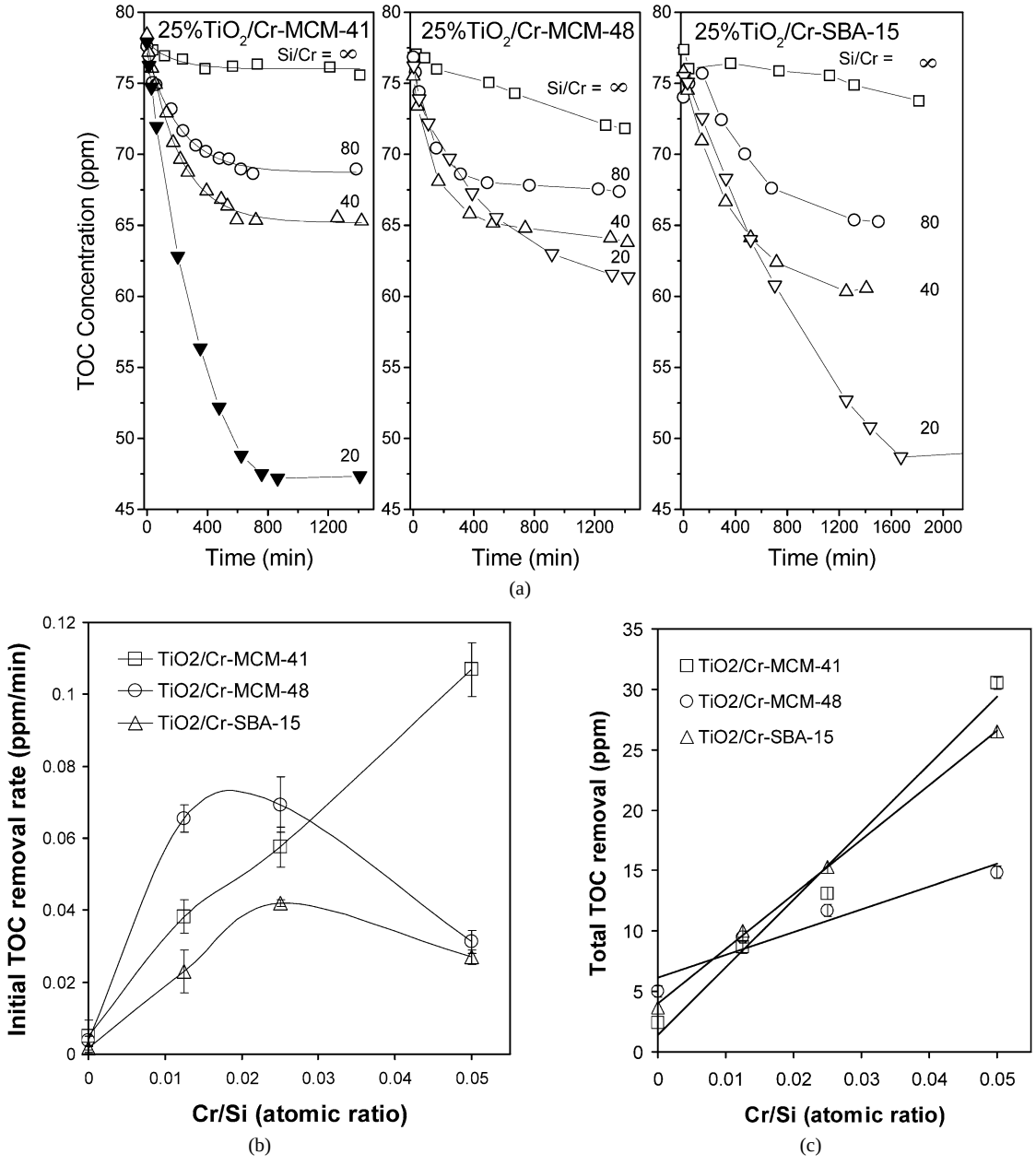

Fig. 8. (a) The time course of TOC concentration during photocatalytic 4-chlorophenol decomposition with 25% TiO_2-loaded Cr-modified MCM-41, MCM-48 and SBA-15. Initial conditions: 1 mM 4-CP, 0.8 g/L catalyst, 25 °C. The corresponding (b) initial TOC removal rate and (c) total TOC destruction ability with respect to Cr/Si ratio.

4. Conclusion

25%TiO_2/Cr-MCM-41 (Si/Cr = 20) is the best visible-light photocatalyst obtained in this study. All of the catalysts can absorb the light with wavelength <550 nm. Cr^{6+} is the form of Cr in Cr-MS and TiO_2/Cr-MS. TPR results indicate that the Si–O–Cr–O–Si bond structure is formed in the MCM-41 matrix, bulk Cr oxide exists outside the MCM-48 matrix, and Cr interacts mainly with silica on the surface of SBA-15. The TiO_2/Cr-MS catalysts deactivate with time during 4-CP photo-oxidation under visible light. The total TOC removal of the catalysts is almost linear to the amount of Cr incorporation with each MS series. The optimum Cr amounts differ for each MS obtained from the standpoint of initial reaction rate. The interaction of TiO_2 and Cr^{6+} is essential for a photocatalyst to be active. The Si–O–Cr bond, which can provide more possibilities for the efficient interaction of TiO_2 and Cr^{6+}, is preferred for achieving a more active photocatalyst, although not necessary.

Acknowledgments

The authors wish to acknowledge the National Science Foundation (NSF) and the US Department of Army for partial support for this work through grants CTS-0097347 and DAAD 19-00-1-0399, respectively. They also acknowledge funding from the Ohio Board of Regents (OBR), which provided matching funds for equipment to NSF grant CTS-9619392 through

the OBR Action Fund 333. The authors thank Lei Ji, Chemical Engineering Department, University of Cincinnati, for synthesizing Cr-MCM-48.

Supplementary material

Supplementary material associated with this article can be found, in the online version, at doi: 10.1016/j.jcat.2005.10.028.

References

[1] M.R. Hoffmann, S.T. Martin, W.Y. Choi, D.W. Bahnemann, Chem. Rev. 95 (1995) 69.
[2] A. Hagfeldt, M. Gratzel, Chem. Rev. 95 (1995) 49.
[3] M.A. Fox, M.T. Dulay, Chem. Rev. 93 (1993) 341.
[4] A.L. Linsebigler, G.Q. Lu, J.T. Yates, Chem. Rev. 95 (1995) 735.
[5] H. Tang, H. Berger, P.E. Schmid, F. Levy, Solid State Commun. 92 (1994) 267.
[6] L. Kavan, M. Gratzel, S. Gilbert, C. Klemenz, H.J. Scheel, J. Am. Chem. Soc. 118 (1996) 6716.
[7] Z.G. Zou, J.H. Ye, K. Sayama, H. Arakawa, Nature 414 (2001) 625.
[8] U. Bach, D. Lupo, P. Comte, J.E. Moser, F. Weissortel, J. Salbeck, H. Spreitzer, Gratzel, M. Nature 395 (1998) 583.
[9] R. Asahi, T. Morikawa, T. Ohwaki, K. Aoki, Y. Taga, Science 293 (2001) 269.
[10] S.U.M. Khan, M. Al-Shahry, W.B. Ingler, Science 297 (2002) 2243.
[11] M. Gratzel, Nature 421 (2003) 586.
[12] L. Zang, C. Lange, I. Abraham, S. Storck, W.F. Maier, H. Kisch, J. Phys. Chem. B 102 (1998) 10765.
[13] L. Davydov, E.P. Reddy, P. France, P.G. Smirniotis, J. Catal. 203 (2001) 157.
[14] E.P. Reddy, L. Davydov, P.G. Smirniotis, J. Phys. Chem. B 106 (2002) 3394.
[15] E.P. Reddy, B. Sun, P.G. Smirniotis, J. Phys. Chem. B 108 (2004) 17198.
[16] B. Sun, E.P. Reddy, P.G. Smirniotis, Appl. Catal. B-Environ. 57 (2005) 139.
[17] Y.M. Xu, C.H. Langford, J. Phys. Chem. 99 (1995) 11501.
[18] Y.M. Xu, C.H. Langford, J. Phys. Chem. B 101 (1997) 3115.
[19] N. Serpone, D. Lawless, J. Disdier, J.M. Herrmann, Langmuir 10 (1994) 643.
[20] W.Y. Choi, A. Termin, M.R. Hoffmann, J. Phys. Chem. 98 (1994) 13669.
[21] J.S. Beck, J.C. Vartuli, W.J. Roth, M.E. Leonowicz, C.T. Kresge, K.D. Schmitt, C.T.W. Chu, D.H. Olson, E.W. Sheppard, S.B. Mccullen, J.B. Higgins, J.L. Schlenker, J. Am. Chem. Soc. 114 (1992) 10834.
[22] J.C. Vartuli, K.D. Schmitt, C.T. Kresge, W.J. Roth, M.E. Leonowicz, S.B. Mccullen, S.D. Hellring, J.S. Beck, J.L. Schlenker, D.H. Olson, E.W. Sheppard, Chem. Mater. 6 (1994) 2317.
[23] D.Y. Zhao, J.L. Feng, Q.S. Huo, N. Melosh, G.H. Fredrickson, B.F. Chmelka, G.D. Stucky, Science 279 (1998) 548.
[24] S. Wang, D. Wu, Y. Sun, B. Zhong, Mater. Res. Bull. 36 (2001) 1717.
[25] Y. Wang, M. Noguchi, Y. Takahashi, Y. Ohtsuka, Catal. Today 68 (2001) 3.
[26] X.Z. Zhang, Y.H. Yue, Z. Gao, Catal. Lett. 83 (2002) 19.
[27] S. Gómez, L.J. Garces, J. Villegas, R. Ghosh, O. Giraldo, S.L. Suib, J. Catal. 233 (2005) 60.
[28] M. Widenmeyer, R. Anwander, Chem. Mater. 14 (2002) 1827.
[29] M. Kruk, M. Jaroniec, C.H. Ko, R. Ryoo, Chem. Mater. 12 (2000) 1961.
[30] J.Y. Ying, C.P. Mehnert, M.S. Wong, Angew. Chem. Int. Ed. 38 (1999) 56.
[31] C. Koepke, K. Wisniewski, M. Grinberg, F. Rozploch, J. Phys.-Condes. Matter. 14 (2002) 11553.
[32] C.S. Turchi, D.F. Ollis, J. Catal. 122 (1990) 178.
[33] K. Okamoto, Y. Yamamoto, H. Tanaka, A. Itaya, Bull. Chem. Soc. Jpn. 58 (1985) 2023.
[34] B. Sun, A.V. Vorontsov, P.G. Smirniotis, Langmuir 19 (2003) 3151.
[35] R.W. Matthews, Water Res. 20 (1986) 569.
[36] C. Koepke, K. Wisniewski, M. Grinberg, A. Majchrowski, T.P.J. Han, J. Phys. Condens. Matter. 13 (2001) 2701.
[37] H. Yamashita, K. Yoshizawa, M. Ariyuki, S. Higashimoto, M. Che, M. Anpo, Chem. Commun. (2001) 435.
[38] H. Yamashita, M. Anpo, Curr. Opin. Solid State. M. 7 (2003) 471.
[39] H. Yamashita, S. Ohshiro, K. Kida, K. Yoshizawa, M. Anpo, Res. Chem. Intermediat. 29 (2003) 881.
[40] S.C. Moon, M. Fujino, H. Yamashita, M. Anpo, J. Phys. Chem. B 101 (1997) 369.
[41] W.S. Ju, M. Matsuoka, K. Iino, H. Yamashita, M. Anpo, J. Phys. Chem. B 108 (2004) 2128.
[42] M. Anpo, S. Higashimoto, M. Matsuoka, N. Zhanpeisov, Y. Shioya, S. Dzwigaj, M. Che, Catal. Today 78 (2003) 211.
[43] J.L. Zhang, M. Minagawa, T. Ayusawa, S. Natarajan, H. Yamashita, M. Matsuoka, M. Anpo, J. Phys. Chem. B 104 (2000) 11501.
[44] R. Tsumura, S. Higashimoto, M. Matsuoka, H. Yamashita, M. Che, M. Anpo, Catal. Lett. 68 (2000) 101.